catalysts

MDPI

Article

Effect of the Type of Heterostructures on Photostimulated Alteration of the Surface Hydrophilicity: $TiO_2/BiVO_4$ vs. $ZnO/BiVO_4$ Planar Heterostructured Coatings

Maria V. Maevskaya [1], Aida V. Rudakova [1], Alexandra V. Koroleva [2], Aleksandr S. Sakhatskii [3], Alexei V. Emeline [1] and Detlef W. Bahnemann [1,4,*]

1 Laboratory "Photoactive Nanocomposite Materials", Saint-Petersburg State University, Ulianovskaya Str. 1, Peterhof, 198504 Saint-Petersburg, Russia; maria.maevskaya@spbu.ru (M.V.M.); aida.rudakova@spbu.ru (A.V.R.); alexei.emeline@spbu.ru (A.V.E.)
2 Centre for Physical Methods of Surface Investigation, Research Park, Saint-Petersburg State University, Ulianovskaya Str. 1, Peterhof, 198504 Saint-Petersburg, Russia; dalika@inbox.ru
3 Centre for Diagnostics of Functional Materials for Medicine, Pharmacology and Nanoelectronics, Research Park, Saint-Petersburg State University, Ulianovskaya Str. 1, Peterhof, 198504 Saint-Petersburg, Russia; ale.x-man@mail.ru
4 Institut fuer Technische Chemie, Gottfried Wilhelm Leibniz Universitaet Hannover, Callinstrasse 3, D-30167 Hannover, Germany
* Correspondence: bahnemann@iftc.uni-hannover.de

Citation: Maevskaya, M.V.; Rudakova, A.V.; Koroleva, A.V.; Sakhatskii, A.S.; Emeline, A.V.; Bahnemann, D.W. Effect of the Type of Heterostructures on Photostimulated Alteration of the Surface Hydrophilicity: $TiO_2/BiVO_4$ vs. $ZnO/BiVO_4$ Planar Heterostructured Coatings. *Catalysts* **2021**, *11*, 1424. https://doi.org/10.3390/catal11121424

Academic Editor: Nicolas Alonso-Vante

Received: 2 November 2021
Accepted: 20 November 2021
Published: 23 November 2021

Abstract: Here, we report the results of comparative studies of the photostimulated hydrophilic behavior of heterostructured $TiO_2/BiVO_4$ and $ZnO/BiVO_4$, and monocomponent TiO_2 and ZnO nanocoating surfaces. The chemical composition and morphology of the synthesized nanocoatings were characterized by XPS, SEM, and AFM methods. The electronic energy structure of the heterostructure components (band gap, top of the valence band, bottom of the conduction band, and Fermi level position) was determined on the basis of experimental results obtained by XPS, UV-V absorption spectroscopy and Kelvin probe methods. According to their electronic energy structure, the $ZnO/BiVO_4$ and $TiO_2/BiVO_4$ heterostructures correspond to type I and type II heterostructures, respectively. The difference in the type of heterostructures causes the difference in the charge transfer behavior at heterojunctions: the type II $TiO_2/BiVO_4$ heterostructure favors and the type I $ZnO/BiVO_4$ heterostructure prevents the photogenerated hole transfer from $BiVO_4$ to the outer layer of the corresponding metal oxide. The results of the comparative studies show that the interaction of the photogenerated holes with surface hydroxy-hydrated multilayers is responsible for the superhydrophilic surface conversion accompanying the increase of the surface free energy and work function. The formation of the type II heterostructure leads to the spectral sensitization of the photostimulated surface superhydrophilic conversion.

Keywords: photostimulated hydrophilicity; metal oxide surfaces; heterostructures; charge transfer; charge separation; heterojunctions; surface energy; work function

1. Introduction

Nowadays, heterostructured photoactive materials are increasingly being used in solar energy harvesting instead of individual semiconductor materials. The combination of two or more different semiconductors in one system improves the spatial separation of photogenerated charge carriers and sensitizes photocatalysts to visible light [1–5].

Depending on the mutual arrangement of the energies of the electronic valence (VB) and conduction (CB) bands of semiconductors, two-component systems can form three different types of heterostructures. These three heterostructures differ in the type and direction of electron and hole transfer at the heterojunctions stimulated by photoexcitation of the entire system or one of its components. This issue is discussed in more detail

elsewhere [6,7]. A review of the literature regarding advances in photocatalysis and photoelectrochemistry shows that the formation of type II heterostructured systems is one of the common methods of increasing the efficiency of photocatalytic and photoelectrochemical systems [1,3,8], due to the charge separation at heterojunctions, which is a distinguished feature of type II heterostructures.

Type II heterostructures are also of greatest interest in the mechanistic study of photoinduced changes in the surface hydrophilicity of "layer-by-layer" films composed of photoactive materials, since effective charge separation leads to the purposeful alteration in the ratio between electron and hole concentrations compared to that of an individual semiconductor. According to the previously proposed mechanism [9,10] of photostimulated alteration of the surface hydrophilicity, this ratio between electron and hole concentrations at the surface is responsible for the direction and efficiency of the effect.

Titanium dioxide and zinc oxide are definitely the best known and most effective photocatalysts; photoactive materials based on these oxides are used to clean wastewater, air, and to create photocells (see for example, [11–17], and references therein). Due to their self-cleaning ability, titanium dioxide and zinc oxide are also the most popular objects for studying photoinduced surface hydrophilicity [11,18,19]. As wide bandgap semiconductors, ZnO and TiO_2 in combination with narrow bandgap semiconductors can easily form types I and II heterostructured systems. A visible-light-induced alteration of the surface hydrophilicity is expected to be observed for such coatings due to the charge separation realizing at heterojunctions.

The photoinduced hydrophilic conversion on TiO_2 or ZnO surfaces has been comprehensively studied for TiO_2/WO_3 [20,21], TiO_2/CdS [22,23], TiO_2/ZnO [10], TiO_2/Cu_2O, and ZnO/Cu_2O [24] layered films. The efficiency of photoinduced superhydrophilic conversion on the titanium dioxide surface increased only in the case of TiO_2/WO_3 films, while CdS, Cu_2O, and *p*-Si [25] substrates inhibited the process rate. These experimental data suggest that photoholes are the carrier responsible for the effect of photoinduced superhydrophilicity of TiO_2. This observation is consistent with the conclusions drawn from the results obtained by other approaches [18,26,27].

Bismuth vanadate is an n-type semiconductor with a band gap energy (E_{bg} = 2.4 eV) lower than that of titania and zinc oxide and corresponds to the absorption of the visible light (wavelengths $\leq$ 515 nm) [28]. The combination of these oxides and $BiVO_4$ has been shown to yield attractive results for the development of semiconductor nanocomposite materials with enhanced visible-light activity in solar to chemical conversion [7,29–32].

This work is aimed at studying the effect of the $BiVO_4$ sublayer on the photostimulated alteration of the surface hydrophilicity of TiO_2 and ZnO coatings. Synthesized planar heterostructured coatings were characterized by X-ray photoelectron spectroscopy (XPS), diffuse reflectance spectroscopy (DRS) and Kelvin probe methods. A comparative analysis of the results of the photoinduced hydrophilic behavior of the surfaces of both heterostructured $TiO_2/BiVO_4$ and $ZnO/BiVO_4$, and monocomponent TiO_2 and ZnO nanocoatings was performed.

2. Results

2.1. Sample Characterization

The formation of coatings with desired compositions, structures, and morphologies was confirmed by XRD, SEM, AFM, and XPS methods (see the Supplementary Materials). XRD patterns of film samples point to the presence of anatase, zincite, and monoclinic clinobisvanite for TiO_2, ZnO, and $BiVO_4$ films, respectively (see Figure S1).

The coatings' surfaces present closely packed nanoparticles with average sizes about 10–15 nm for TiO_2-topped coatings and about 15–20 nm for ZnO-topped coatings (see SEM images in Figures S2 and S3). The average roughness (Ra) of the coating surfaces does not exceed $\pm$6 nm (see AFM data in Figures S4 and S5), which indicates sufficient surface smoothness so as not to affect the hydrophilicity of the surface. All characteristics of the prepared nanocoatings are listed in Table 1.

Table 1. The samples characterization.

Coating	Crystalline Phase	Thickness, nm	Average Particle Diameter, nm	Ra, nm
TiO_2	anatase	50	15	±1
$TiO_2/BiVO_4$	anatase/monoclinic	50/50	10	±5
ZnO	zincite	80	15	±3
$ZnO/BiVO_4$	zincite/monoclinic	70/50	20	±6

2.2. Electronic Properties of the Heterostructure Components

The bandgap energy values (E_{bg}) were determined using the transmittance spectra of nanocoatings modified by a Tauc plot approach (see Figure S6). The estimated E_{bg} values are listed in Table 2.

Table 2. Positions of the conduction and valence bands and band gap energies of the coating components with respect to vacuum energy level.

Coating Component	E_{bg}, eV	E_F, eV	E_{VB}, eV	E_{CB}, eV
TiO_2	3.2	−5.1	−7.2	−3.9
ZnO	3.3	−5.4	−8.0	−4.7
$BiVO_4$	2.5	−6.0	−7.4	−4.9

The work function characteristics (E_F) of the nanocoatings were measured by the Kelvin probe method. They correspond to the positions of the Fermi levels.

XPS spectra recorded in the low binding energy region (see Figure S7) were used to recognize the valence band positions (E_{VB}) of the components of heterostructured coatings. Corresponding values with respect to the vacuum energy level are given in Table 2.

For each coating component, the energy level of the conduction band bottom (E_{CB}) was calculated as a sum of the energies corresponding to the valence band top and optical band gap (see Table 2):

$$E_{CB} = E_{VB} + E_{bg} \quad (1)$$

2.3. Photoinduced Alterations in Surface Hydrophilicity of Heterostructured Coatings

The effect of irradiation on the surface hydrophilicity of nanocoatings was studied for strongly hydrated surface. This state of the surface is well reproducible and considered as the initial surface state for further kinetic studies of light-induced changes of surface hydrophilicity as a function of irradiation time. The hydrophilicity of this state is characterized by initial water contact angle values of 35–43° for TiO_2 and $TiO_2/BiVO_4$, and 23–25° for ZnO and $ZnO/BiVO_4$ coatings, respectively (Figures 1 and 2). In parallel with the kinetic WCA measurements, the corresponding values of the work function and surface free energy depending on the spectral range of the acting light were determined for all coatings (Tables 3 and 4, Figure 3).

Table 3. Work function values (WF) after different treatments for all studied coatings.

Coating	WF, eV (±0.02 eV)			
	As Prepared	Wetted	UV-Irradiated	Vis-Irradiated
$BiVO_4$	6.02	5.14	4.95	4.83
TiO_2	5.10	4.65	5.19	4.63
$TiO_2/BiVO_4$	5.56	5.17	5.26	5.36
ZnO	5.40	5.18	5.29	5.00
$ZnO/BiVO_4$	5.69	5.09	5.22	4.94

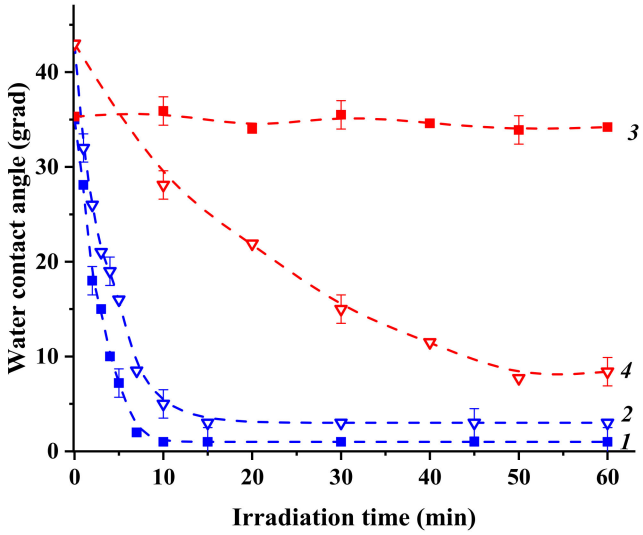

Figure 1. Kinetics of the water contact angle alterations for TiO_2 (*1*, *3*) and $TiO_2/BiVO_4$ (*2*, *4*) coatings under UV (*1*, *2*) and visible (*3*, *4*) light irradiation. The error on the water contact angle measurement was ±1.5° for all data sets (presented as bars).

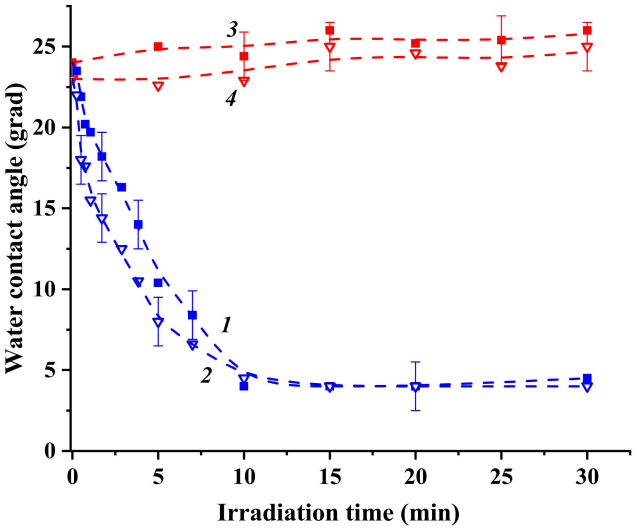

Figure 2. Kinetics of the water contact angle alterations for ZnO (*1*, *3*) and $ZnO/BiVO_4$ (*2*, *4*) coatings under UV (*1*, *2*) and visible (*3*, *4*) light irradiation. The error on the water contact angle measurement was ±1.5° for all data sets (presented as bars).

Table 4. Total (t), polar (p), and dispersive (d) surface free energie (SFE) values for all coatings studied after different treatments.

Coating	SFE, mN/m (±0.02 eV)								
	Wetted			UV-Irradiated			Vis-Irradiated		
	t	d	p	t	d	p	t	d	p
TiO_2	65.7	39.6	26.1	79.8	47.6	32.2	67.0	40.1	26.8
$TiO_2/BiVO_4$	62.0	40.1	21.9	80.1	48.1	32.0	77.8	44.2	33.6
ZnO	77.8	44.2	33.6	80.8	50.0	30.8	74.1	47.2	26.9
$ZnO/BiVO_4$	76.1	46.8	29.3	80.8	49.9	30.9	75.0	48.3	26.7

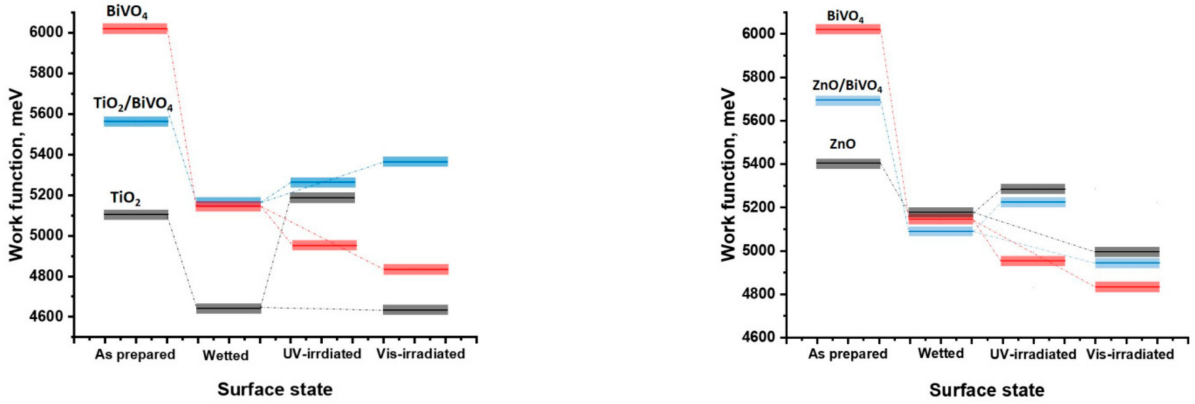

Figure 3. Evolution of the work function values for heterostructured coatings and their components depending on the treatment type: (**a**) $TiO_2/BiVO_4$, TiO_2, and $BiVO_4$, (**b**) $ZnO/BiVO_4$, ZnO, and $BiVO_4$.

The light-induced hydrophilic behavior of the $TiO_2/BiVO_4$ heterosystem is significantly different compared to the monocomponent TiO_2 film (Figure 1, curves *2* and *1*). Upon UV irradiation, its surface state turns into the superhydrophilic state with a lower efficiency with respect to that of the individual film. Exposure of the $TiO_2/BiVO_4$ coating to visible light also leads to an increase in hydrophilicity, reaching the value of 7° (superhydrophilicity) after 1 h of irradiation, while the hydrophilic surface state of the TiO_2 coating remains unchanged within the experimental error (Figure 1, curves *4* and *3*).

Figure 2 shows the kinetic dependences of the photoinduced WCA alterations for the $ZnO/BiVO_4$ heterostructured coating and corresponding monocomponent ZnO coating. UV-induced superhydrophilic conversion is observed on the surfaces of the heterostructured $ZnO/BiVO_4$ as well as monocomponent ZnO coatings (curves *2* and *1*). At the same time, the surface hydrophilicity of both coatings does not undergo any changes within the WCA error limits when irradiated with visible light (curves *3* and *4*). Thus, no significant differences were found in the kinetic dependences of the water contact angle under UV and visible light irradiation for surfaces of both ZnO and $ZnO/BiVO_4$ planar systems.

Table 3 shows the work function values for monocomponent and heterostructured coatings after surface hydration ("wetted") and after irradiation of the surface with light of different spectral composition ("UV-irradiated" and "Vis-irradiated"). To demonstrate the direction of the photoinduced alteration of the work function values for all the films studied, the data are graphically presented in Figure 3.

The strong surface hydration of the TiO_2 and ZnO layers reduces the work function values for all the samples studied (Figure 3). For UV-irradiated surfaces of all planar systems, the work function values increase compared to their initial values for the wetted state. This observation corresponds to the photoinduced superhydrophilic state of their surfaces (Figures 1 and 2).

The effects induced by visible light irradiation of the coating surfaces depend on the coating composition. The monocomponent TiO_2 and heterostructured $TiO_2/BiVO_4$ coatings demonstrate different trends in the alteration of the work function under visible light irradiation. As shown in Figure 3a, the work function of TiO_2 practically does not change, while the WF of the $TiO_2/BiVO_4$ heterosystem increases. These visible light-driven alterations of WFs correlate with the different Vis-induced hydrophilic behavior of the TiO_2 surface for individual and heterostructured coatings (Figure 1).

The work functions for both ZnO and $ZnO/BiVO_4$ coatings decrease slightly when exposed to visible light and are very close in value (Figure 3b). Thus, the UV- and visible-light-induced WF changes are similar in directions and values for both ZnO and $ZnO/BiVO_4$ planar systems. Thus, the trends of WF alterations also quantitatively correlate with their UV- and Vis-induced hydrophilicity changes (Figure 2).

Table 4 presents data on the total surface free energy (SFE), and its dispersive and polar components, for the surface of all systems studied.

The UV-stimulated WCA change for the surface of the monocomponent TiO_2 coating is caused by an SFE increase mainly due to its polar component. Upon visible light irradiation, no significant deviations were observed in both the SFE value (Table 4) and surface hydrophilicity (Figure 1). The transformation of the $TiO_2/BiVO_4$ heterostructured coating surface into a more hydrophilic state under UV irradiation as well as visible light is accompanied by an increase in SFE due to both components. However, the increase in the polar component contributes more to the alteration of the total surface free energy when the $TiO_2/BiVO_4$ sample was exposed to visible light.

For the ZnO and $ZnO/BiVO_4$ coatings, the UV-induced surface transition to the superhydrophilic state is characterized by an increase in the total surface energy to a value of 80.8 mN/m, mainly due to its dispersive component (Table 4). When both systems are irradiated with visible light, their surface energy slightly decreases, mainly due to the polar component.

3. Discussion

Based on the experimental results on the determination of the electronic bands positions in the components (see the data in Table 2) of the formed heterostructures, the corresponding energy diagram can be plotted as shown in Figure 4. A successful formation of heterojunctions in heterostructured coatings is confirmed by the alteration of their work functions (Fermi level positions) comparing to the corresponding parameters for the individual components (see the data presented in Tables 2 and 3): the work function values of both heterostructured coatings are located between the corresponding values of the individual components, which indicates the charge separation at heterojunctions. The wetting of the surfaces of both heterostructured and monocomponent coatings results in a decrease of the work function values due to the formation of the hydroxy-hydrated multilayers [9,33].

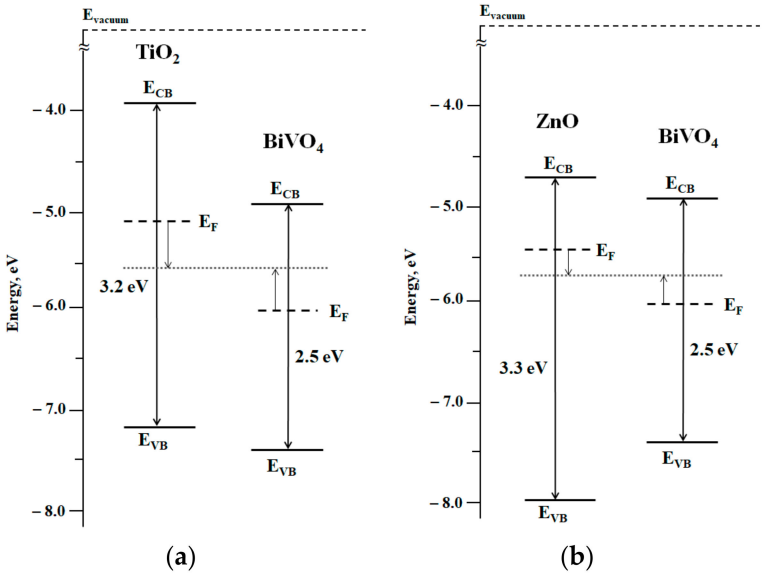

Figure 4. Energy diagrams of the positions of the top of the valence bands and the bottom of the conduction bands and Fermi level positions for TiO_2 and $BiVO_4$ (**a**) and ZnO and $BiVO_4$ (**b**) heterosystems.

According to the energy diagrams, the heterostructure formed from TiO_2 and $BiVO_4$ corresponds to type II and the energy levels of conduction and valence bands of its components favor the photogenerated electron transfer from TiO_2 to $BiVO_4$ and the photogenerated hole transfer back from $BiVO_4$ to TiO_2. As a result, the charge separation at

heterojunctions in such types of heterostructure results in hole accumulation in TiO_2, and accordingly, at the surface of the heterostructured coating. At the same time, the mutual positions of the conduction and valence bands of ZnO and $BiVO_4$ indicate that the corresponding ZnO–$BiVO_4$ heterostructure belongs to type I, which means that both photogenerated electrons and holes are transferred from ZnO to $BiVO_4$. Thus, there is no charge separation at heterojunctions occurring in such a heterostructure and therefore, there is no alteration of the dominating charge carriers at the surface of the heterostructured coating compared to the monocomponent ZnO coating. The possibility of forming a type I heterostructure for the ZnO/$BiVO_4$ heterosystem and a type II heterostructure for the TiO_2/$BiVO_4$ heterosystem has been mentioned earlier [7,29–32,34–36].

The corresponding processes of the charge transfer and separation of photogenerated charge carriers at heterojunctions are shown for the TiO_2/$BiVO_4$ heterostructure in Figure 5 and for the ZnO/$BiVO_4$ heterostructure in Figure 6, respectively. Note that in the TiO_2/$BiVO_4$ heterostructure of type II, the accumulation of photogenerated holes occurred at the TiO_2 surface under both UV and visible light photoexcitation, corresponding to a photoexcitation of both components and $BiVO_4$ only, respectively. At the same time, regardless of the type of photoexcitation there is no charge transfer process to the ZnO component due to the energy barrier for both electrons and holes preventing the charge carrier transfer from ZnO to $BiVO_4$. Thus, the photoexcitation of the ZnO/$BiVO_4$ heterostructure of type I does not change the dominating type of the charge carrier at the ZnO surface.

The difference in charge transfer processes taking place at heterojunctions of type I ZnO/$BiVO_4$ and type II TiO_2/$BiVO_4$ heterostructures explains the difference in the photostimulated surface hydrophilic behavior of both heterostructures. An accumulation of holes at the TiO_2 surface due to charge separation at the heterojunction in the type II TiO_2/$BiVO_4$ heterostructure takes place and results in a surface transition to superhydrophilic state under both UV and visible light photoexcitation. However, both UV and visible light photoexcitation of the type I ZnO/$BiVO_4$ heterostructure does not lead to the interface transfer of either electrons or holes from $BiVO_4$ to ZnO and therefore, does not change the dominating type of the charge carriers at the ZnO surface. Accordingly, the behavior of the ZnO surface in heterostructured coatings remains similar to that one observed for the monocomponent ZnO surface.

It is wise to mention that the photostimulated transition of the coating surface to the superhydrophilic state corresponds to an increase of the work function regardless of the coating structure, either monocomponent or heterostructured (see data in Table 3 and Figure 3). This accordance between surface hydrophilicity and work function values can be explained in terms of the interaction between the photogenerated holes and the surface hydroxy-hydrated layer, which changes the surface dipole moment affecting the work function value.

The interaction between photogenerated holes as a dominating type of the charge carriers at the surface and hydroxy-hydrated multilayers also results in an increase of the surface free energy (see data in Table 4), mainly its polar component. This also indicates that such a reconstruction process occurred in the hydroxy-hydrated multilayer so that the surface reached a superhydrophilic state. Thus, there is a qualitative correlation between work function, surface free energy, and surface hydrophilicity.

It is also wise to mention that the formation of the heterostructured coatings with type II heterojunctions favorable to hole transfer toward the outer component surface (Figure 6b) leads to a spectral sensitization to visible light of the photostimulated superhydrophilicity effect.

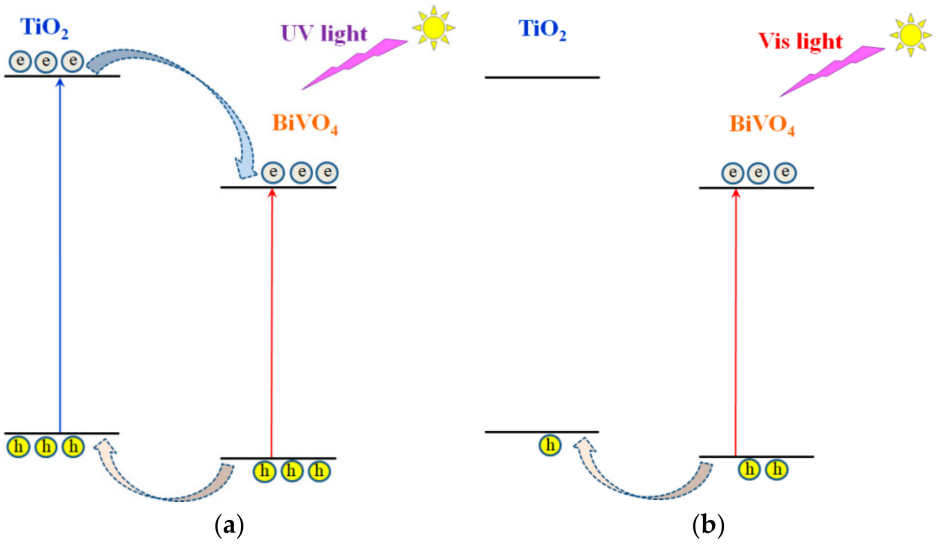

Figure 5. Schemes of the electron transfer in heterostructured $TiO_2/BiVO_4$ coating under UV (**a**) and visible (**b**) light photoexcitation.

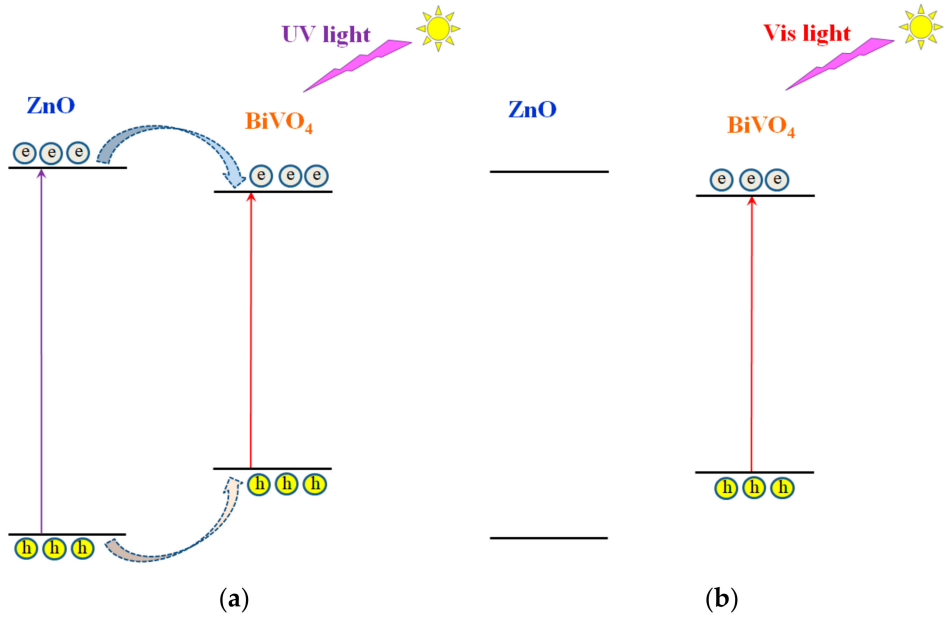

Figure 6. Schemes of the electron transfer in heterostructured $ZnO/BiVO_4$ coating under UV (**a**) and visible (**b**) light photoexcitation.

4. Materials and Methods

The individual TiO_2 and ZnO films were prepared from their individual sols using a dip coating method (KSV Nima dip coater, Espoo, Finland). All films studied were deposited on SiO_2-coated glass substrates to prevent the diffusion of sodium ions from the glass during its thermal treatment [37,38].

To prepare titanium dioxide sol, 40 mL of titanium (IV) isopropoxide (99.999%, Sigma Aldrich, Moscow, Russia) was added to 120 mL of isopropanol (99.8%, Ecos-1, Moscow, Russia) and intensively stirred for 2 h at room temperature. The velocity of withdrawing from solution was 50 mm/min. The deposited thin TiO_2 layers were annealed at 450 °C for 1 h in ambient atmosphere [39].

For the zinc oxide sol, 2.5 mL of ethylene glycol (99.5%, LenReactiv, Saint-Petersburg, Russia) and 10 g of zinc acetate dihydrate $Zn(OAc)_2 \cdot 2H_2O$ (99.0%, Vekton, Saint-Petersburg, Russia) were mixed in a round-bottomed flask and heated at 70 °C for 15 min to obtain a

uniform transparent mixture. After cooling to room temperature, 150 mL of isopropanol (99.8%, Ecos-1, Moscow, Russia) and 6.4 mL of triethylamine (99.5%, PanReac AppliChem, Darmstadt, Germany) were added to the mixture to promote the hydrolysis of the zinc acetate [24]. To improve the quality of the film, 0.5 mL of glycerol (99.5%, LenReactiv, Saint-Petersburg, Russia) was added dropwise. The obtained clear and homogeneous solution previously stirred at 60 °C for 1 h aged for 24 h at room temperature. Thin ZnO films were obtained by two dips in the solution at a withdrawal rate of 100 mm/min and with intermediate drying at 100 °C for 15 min. Then, films were annealed at 300 °C for 1 h in ambient atmosphere.

The $BiVO_4$ films were deposited on SiO_2-coated glass substrates by drop-casting method using a precursor solution. For preparation of the precursor solution, 0.5 mmol bismuth nitrate pentahydrate $Bi(NO_3)_3{\cdot}5H_2O$ (99%, Chemcraft Ltd., Kaliningrad, Russia) and 0.46 mmol vanadyl acetylacetonate $VO(C_5H_7O_2)_2$ (98%, Sigma Aldrich, Moscow, Russia) were dissolved in a mixture of 5 mL glacial acetic acid (≥99%, LenReactiv, Saint-Petersburg, Russia) and 0.25 mL acetylacetone (99%, AlfaAesar, Haverhill, MA, USA) with constant stirring for 1 h. The solution was drop-cast onto the glass substrates (7.5 μL per cm^2). The samples were then dried at 80 °C for 30 min in a vacuum drying oven and finally annealed in a muffle furnace at 450 °C for 1 h under ambient conditions.

The "layer-by-layer" $TiO_2/BiVO_4$ and $ZnO/BiVO_4$ heterosystems were formed by deposition of TiO_2 and ZnO layers, respectively, on a thin $BiVO_4$ film by the methods described above. To demonstrate the 100% coverage of the $BiVO_4$ layer with TiO_2 or ZnO layers, the survey XPS spectra of the heterostructured coatings as well as those of the $BiVO_4$ film for comparison are presented in the Supplementary Materials Section (Figure S8). No peaks related to $BiVO_4$ were found there.

As a result, monocomponent TiO_2 and heterostructured $TiO_2/BiVO_4$ TiO_2-topped coatings as well as monocomponent ZnO and heterostructured $ZnO/BiVO_4$ ZnO-topped coatings were synthesized and studied in this work.

The surface morphology and film thickness of all synthesized films were explored by scanning electron microscopy (Zeiss Supra 40 VP system, Oberkochen, Germany). The average roughness (Ra) of the film surface was assessed by the AFM method using the NOVA 1.0.26 program. X-ray diffraction measurements with Bruker "D8 DISCOVER" high-resolution diffractometer (CuKa X-ray radiation, within the angle range of $20° \leq 2\theta \leq 80°$ with a scanning speed of 5.0°/min, Germany) were used for the crystal phase determination. Structural reference data were taken from the ICSD database. The transmittance spectra were recorded in the 250–800 nm spectral range at ambient conditions using a Lambda 650S spectrophotometer. The XPS spectra were recorded using a Thermo Fisher Scientific Escalab 250Xi spectrometer (Thermo Scientific™, Waltham, MA, USA).

Work function measurements were performed with a scanning Kelvin probe system SKP5050 (KP Technology, Wick, Scotland) versus a golden reference probe electrode (probe area 2 mm^2). The probe oscillation frequency was 74 Hz, and the backing potential was 7000 mV. Work function values were obtained by averaging 50 data points for five different sites of each sample. The error of the work function (WF) measurements was ±0.02 eV.

The contact angle values were measured using optical tensiometer (Bioline Theta Lite, Gothenburg, Sweden). Ultrapure water has initial pH of 5.5. The error of the water contact angle (WCA) measurements was ±1.5°. The surface free energy (SFE) was calculated by the Owens–Wendt–Rabel–Kaelble (OWRK)/Fowkes approach using the two-liquid method (water contact angle versus methylene iodide contact angle) [24].

The work function and contact angle values were measured after each step of the following surface pretreatment procedure. After annealing at 300 °C for 30 min, the state of the film surface was designated as "as prepared". After the storage in the dark in a humid atmosphere for 10 days, the surface state was denoted as "wetted". The third step was to irradiate the film with UV or visible light, and the corresponding surface states were referred to as "UV-irradiated" or "Vis-irradiated", respectively.

The irradiation of the films by UV or visible light was carried out using Xenon lamp (LOMO, Saint-Petersburg, Russia) equipped with a water filter and either UV bandpass or vis cutoff color filter. The transmittance spectra of employed filters are presented in the Supplementary Materials Section (Figure S9). The irradiance of the UV irradiation was 15.0 mW/cm^2 and the irradiance of the visible light irradiation was 225.0 mW/cm^2. The kinetics of the photoinduced water contact angle alteration is presented as a dependence of the water contact angle on the irradiation time.

5. Conclusions

We have conducted a comparative study of the photostimulated processes affecting surface hydrophilicity for type I ZnO/$BiVO_4$ and type II TiO_2/$BiVO_4$ heterostructured coatings. Our results indicate that the type I ZnO/$BiVO_4$ heterostructure does not significantly change the surface behavior of the ZnO surface compared to the surface of the monocomponent ZnO coating. In turn, the type II TiO_2/$BiVO_4$ heterostructure demonstrates a spectral sensitization to the visible light of the photostimulated superhydrophilicity effect, which is not observed for the monocomponent TiO_2 coating. The difference between the two types of heterostructures can be explained in terms of either a realization or prevention of the hole transfer through the heterojunctions toward the outer surface of the heterostructured coatings.

Regardless of the type of coatings, a quantitative correlation between the surface transition to the superhydrophilic state and the increase of both work function and surface free energy values was observed. These correlations indicate the interaction of the holes with the hydroxy-hydrated multilayer at the surface of nanocoatings.

Supplementary Materials: The following are available online at https://www.mdpi.com/article/10.3390/catal11121424/s1, Figure S1: XRD patterns of TiO_2, ZnO, $BiVO_4$, TiO_2/$BiVO_4$, and ZnO/$BiVO_4$ coatings, Figure S2: SEM images of TiO_2-topped surfaces and cross-sections for TiO_2 and TiO_2/$BiVO_4$ coatings, Figure S3: SEM images of ZnO surfaces and cross-sections for ZnO and ZnO/$BiVO_4$ coatings, Figure S4: AFM image of the TiO_2 surfaces and roughness profiles for TiO_2 and TiO_2/$BiVO_4$ coatings., Figure S5: AFM image of the ZnO surfaces and roughness profiles for ZnO and ZnO/$BiVO_4$ coatings, Figure S6: Transmittance spectra and Tauc plots for TiO_2, ZnO, and $BiVO_4$, Figure S7: XPS spectra of valence band region for TiO_2, ZnO, and $BiVO_4$, Figure S8: Transmittance spectra of UV bandpass and Vis cutoff filters, Figure S9: Transmittance spectra of UV band-pass (1) and Vis cut-off (2) filters (Vavilov SOI, Russia).

Author Contributions: Conceptualization, A.V.R. and D.W.B.; methodology, A.V.E.; software, M.V.M.; validation, A.V.R. and A.V.E.; formal analysis, M.V.M.; investigation, M.V.M., A.V.K., A.S.S. and A.V.E.; resources, D.W.B.; writing—original draft preparation, M.V.M., A.V.R. and A.V.E.; writing—review and editing, A.V.E. and D.W.B.; visualization, M.V.M., A.V.R.; supervision, D.W.B.; project administration, A.V.E.; funding acquisition, A.V.E. and D.W.B. All authors have read and agreed to the published version of the manuscript.

Funding: The reported study was funded by RFBR, project number 19-32-90111.

Data Availability Statement: Data is contained within the article and Supplementary Material.

Acknowledgments: AVE and MVM are grateful to the Russian Foundation for Basic Research (RFBR) for grant N 19-32-90111 to support this research. Experimental studies were performed in the laboratory "Photoactive nanocomposite materials" supported by the Saint-Petersburg State University (ID: 73032813). The authors are thankful to the Resource Center (RC) "Nanophotonics", RC "X-ray Diffraction Studies", RC "Centre for Innovative Technologies of Composite Nanomaterials", RC "Centre for Physical Methods of Surface Investigation", RC "Centre for Diagnostics of Functional Materials for Medicine, Pharmacology and Nanoelectronics" and RC "Nanotechnology" of the Research Park at the Saint-Petersburg State University for helpful assistance in the preparation and characterization of the samples.

Conflicts of Interest: The authors declare no conflict of interest.

References

1. Wang, H.; Zhang, L.; Chen, Z.; Hu, J.; Li, S.; Wang, Z.; Liu, J.; Wang, X. Semiconductor heterojunction photocatalysts: Design, construction, and photocatalytic performances. *Chem. Soc. Rev.* **2014**, *43*, 5234–5244. [CrossRef] [PubMed]
2. Emeline, A.V.; Rudakova, A.V.; Mikhaylov, R.V.; Ryabchuk, V.K.; Serpone, N. Electron transfer processes in heterostructured photocatalysts. In *Springer Handbook of Inorganic Photochemistry*, 1st ed.; Bahnemann, D., Patrocinio, A.O.T., Eds.; Springer: Basel, Switzerland, 2022; in press. [CrossRef]
3. Marschall, R. Semiconductor composites: Strategies for enhancing charge carrier separation to improve photocatalytic activity. *Adv. Funct. Mater.* **2013**, *24*, 2421–2440. [CrossRef]
4. Wang, Y.; Wang, Q.; Zhan, X.; Wang, F.; Safdara, M.; He, J. Visible light driven type II heterostructures and their enhanced photocatalysis properties: A review. *Nanoscale* **2013**, *5*, 8326–8339. [CrossRef] [PubMed]
5. Chiu, Y.-H.; Chang, T.-F.M.; Chen, C.-Y.; Sone, M.; Hsu, Y.-J. Mechanistic insights into photodegradation of organic dyes using heterostructure photocatalysts. *Catalysts* **2019**, *9*, 430. [CrossRef]
6. He, X.; Zhang, C. Recent advances in structure design for enhancing photocatalysis. *J. Mater. Sci.* **2019**, *54*, 8831–8851. [CrossRef]
7. Moniz, S.J.A.; Shevlin, S.A.; Martin, D.J.; Guo, Z.-X.; Tang, J. Visible-light driven heterojunction photocatalysts for water splitting—A critical review. *Energy Environ. Sci.* **2015**, *8*, 731–759. [CrossRef]
8. Emeline, A.V.; Rudakova, A.V.; Mikhaylov, R.V.; Bulanin, K.M.; Bahnemann, D.W. Photoactive heterostructures: How they are made and explored. *Catalysts* **2021**, *11*, 294. [CrossRef]
9. Rudakova, A.V.; Emeline, A.V. Photoinduced hydrophilicity of surfaces of thin film. *Colloid J.* **2021**, *83*, 20–48. [CrossRef]
10. Rudakova, A.V.; Emeline, A.V.; Bahnemann, D.W. Effect of the TiO_2–ZnO heterostructure on the photoinduced hydrophilic conversion of TiO_2 and ZnO Surfaces. *J. Phys. Chem. C* **2019**, *123*, 8884–8891. [CrossRef]
11. Fujishima, A.; Rao, T.N.; Tryk, D.N. Titanium dioxide photocatalysis. *J. Photochem. Photobiol. C* **2000**, *1*, 1–21. [CrossRef]
12. Chen, X.; Mao, S.S. Titanium dioxide nanomaterials: synthesis, properties, modifications, and applications. *Chem. Rev.* **2007**, *107*, 2891–2959. [CrossRef]
13. Henderson, M.A. A surface science perspective on TiO_2 photocatalysis. *Surf. Sci. Rep.* **2011**, *66*, 185–297. [CrossRef]
14. Carp, O.; Huisman, C.L.; Reller, A. Photoinduced reactivity of titanium dioxide. *Prog. Solid State Chem.* **2004**, *32*, 33–177. [CrossRef]
15. Lee, K.M.; Lai, C.W.; Ngai, K.S.; Juan, J.C. Recent developments of zinc oxide based photocatalyst in water treatment technology: A review. *Water Res.* **2016**, *88*, 428–448. [CrossRef] [PubMed]
16. Ong, C.B.; Ng, L.Y.; Mohammad, A.W. A review of ZnO nanoparticles as solar photocatalysts: Synthesis, mechanisms and applications. *Renew. Sustain. Energy Rev.* **2018**, *81*, 536–551. [CrossRef]
17. Zhang, H.; Chen, G.; Bahnemann, D.W. Photoelectrocatalytic materials for environmental applications. *J. Mater. Chem.* **2009**, *19*, 5089–5121. [CrossRef]
18. Sun, R.-D.; Nakajima, A.; Fujishima, A.; Watanabe, T.; Hashimoto, K. Photoinduced surface wettability conversion of ZnO and TiO_2 thin films. *J. Phys. Chem. B* **2001**, *105*, 1984–1990. [CrossRef]
19. Miyauchi, M.; Nakajima, A.; Watanabe, T.; Hashimoto, K. Photocatalysis and photoinduced hydrophilicity of various metal oxide thin films. *Chem. Mater.* **2002**, *14*, 2812–2816. [CrossRef]
20. Miyauchi, M.; Nakajima, A.; Watanabe, T.; Hashimoto, K. Photoinduced hydrophilic conversion of TiO_2/WO_3 layered thin films. *Chem. Mater.* **2002**, *14*, 4714–4720. [CrossRef]
21. Kim, H.-M.; Kim, D.; Kim, B. Photoinduced hydrophilicity of TiO_2/WO_3 double layer films. *Surf. Coat. Technol.* **2015**, *271*, 18–21. [CrossRef]
22. Maevskaya, M.V.; Sivokhina, M.M.; Rudakova, A.V.; Emeline, A.V. Photocatalytic properties of layered TiO_2/CdS, TiO_2/ZnO, ZnO/TiO_2 heterostructures. In Proceedings of the 6th International Conference on Semiconductor and Photochemistry, Oldenburg, Germany, 11–14 September 2017.
23. Grishina, A.E.; Maevskaya, M.V.; Rudakova, A.V.; Emeline, A.V. Photoinduced hydrophilic behavior of hydrated surfaces of TiO_2/ZnO, TiO_2/CdS, TiO_2/WO_3 composite films. In Proceedings of the 9th European Meeting on Solar Chemistry and Photocatalysis, Strasburg, France, 13–17 June 2016.
24. Maevskaya, M.V.; Rudakova, A.V.; Emeline, A.V.; Bahnemann, D.W. Effect of Cu_2O substrate on photoinduced hydrophilicity of TiO_2 and ZnO nanocoatings. *Nanomaterials* **2021**, *11*, 1526. [CrossRef] [PubMed]
25. Rudakova, A.V.; Emeline, A.V.; Romanychev, A.I.; Bahnemann, D.W. Photoinduced hydrophilic behavior of TiO_2 thin film on Si substrate. *J. Alloy. Compd.* **2021**, *872*, 159746. [CrossRef]
26. Fujishima, A.; Zhang, X. Titanium dioxide photocatalysis: Present situation and future approaches. *Comptes Rendus Chim.* **2006**, *9*, 750–760. [CrossRef]
27. Fujishima, A.; Zhang, X.; Tryk, D.A. TiO_2 photocatalysis and related surface phenomena. *Surf. Sci. Rep.* **2008**, *63*, 515–582. [CrossRef]
28. Samsudin, M.F.R.; Sufian, S.; Hameed, B.H. Epigrammatic progress and perspective on the photocatalytic properties of $BiVO_4$-based photocatalyst in photocatalytic water treatment technology: A review. *J. Mol. Liq.* **2018**, *268*, 438–459. [CrossRef]
29. Wetchakun, N.; Chainet, S.; Phanichphant, S.; Wetchakun, K. Efficient photocatalytic degradation of methylene blue over $BiVO_4/TiO_2$ nanocomposites. *Ceram. Int.* **2015**, *41*, 5999–6004. [CrossRef]

30. Qian, B.; Xu, Q.; Wu, Y.; Zhang, Y.; Li, H.; Wang, Y.; Wang, B.; Li, S.; Song, X.-M. A highly efficient photocatalytic methanol fuel cell based on non-noble metal photoelectrodes: Study on its energy band engineering via experimental and density functional theory method. *J. Power Sources* **2020**, *78*, 228756. [CrossRef]
31. Hu, K.; Lei, E.; Li, Y.; Zhao, X.; Zhao, D.; Zhao, W.; Rong, H. Photocatalytic degradation mechanism of the visible-light responsive $BiVO_4/TiO_2$ core–shell heterojunction photocatalyst. *J. Inorg. Organomet. Polym.* **2020**, *30*, 775–788. [CrossRef]
32. Balachandran, S.; Prakash, N.; Thirumalai, K.; Muruganandham, M.; Sillanpaa, M.; Swaminathan, M. Facile construction of heterostructured $BiVO_4-ZnO$ and its dual application of greater solar photocatalytic activity and self-cleaning property. *Ind. Eng. Chem. Res.* **2014**, *53*, 8346–8356. [CrossRef]
33. Rudakova, A.V.; Oparicheva, U.G.; Grishina, A.E.; Murashkina, A.A.; Emeline, A.V.; Bahnemann, D.W. Photoinduced hydrophilic conversion of hydrated ZnO surfaces. *J. Colloid Interface Sci.* **2016**, *466*, 452–460. [CrossRef]
34. Mohamed, N.A.; Safaei, J.; Ismail, A.F.; Khalid, M.N.; Jailani, M.F.A.M.; Noh, M.F.M.; Arzaee, N.A.; Zhou, D.; Sagu, J.S.; Teridi, M.A.M. Boosting photocatalytic activities of $BiVO_4$ by creation of g-C_3N_4/ZnO@ $BiVO_4$ heterojunction. *Mater. Res. Bull.* **2020**, *125*, 110779. [CrossRef]
35. Zhang, J.; Xie, L. Synthesis and sonophotocatalytic activities of ZnO\$BiVO_4$\$Co_3O_4$ composites. *Chem. Phys. Lett.* **2021**, *775*, 138660. [CrossRef]
36. Zhang, H.; Chen, Y.; Liang, Y. Lotus Leaf-inspired hydrothermal synthesis of composite nanoparticles and application for photocatalytic oil denitrification. *Catal. Lett.* **2020**, *150*, 2474–2486. [CrossRef]
37. Watanabe, T.; Fukayama, S.; Miyauchi, M.; Fujishima, A.; Hashimoto, K. Photocatalytic activity and photo-induced wettability conversion of TiO_2. Thin film prepared by sol-gel process on a soda-lime glass. *J. Sol-Gel Sci. Technol.* **2000**, *19*, 71–76. [CrossRef]
38. Yu, J.; Zhao, X. Effect of substrates on the photocatalytic activity of nanometer TiO_2 thin films. *Mater. Res. Bull.* **2000**, *35*, 1293–1301. [CrossRef]
39. Emeline, A.V.; Rudakova, A.V.; Sakai, M.; Murakami, T.; Fujishima, A. Factors affecting UV-induced superhydrophilic conversion of a TiO_2 surface. *J. Phys. Chem. C* **2013**, *117*, 12086–12092. [CrossRef]